ELSEVIER

Journal of Electroanalytical Chemistry 456 (1998) 25–35

JOURNAL OF ELECTROANALYTICAL CHEMISTRY

An exponentially expanding mesh ideally suited to the fast and efficient simulation of diffusion processes at microdisc electrodes. 3. Application to voltammetry.

D.J. Gavaghan *

Oxford University Computing Laboratory, Wolfson Building, Parks Rd., and Nuffeld Department of Anaesthetics, University of Oxford, Radcliffe Infirmary, Oxford, UK

Received 4 August 1997; received in revised form 21 April 1998

Abstract

In the first paper in this series we derived an exponentially expanding mesh designed specifically to give a fast, efficient solution to the problem of simulation of diffusion processes at microdisc electrodes to a pre-determined level of accuracy. In this paper we make use of this mesh to consider the problem of linear sweep voltammetry and show that for the simulated values of the peak current for a fully reversible reaction we can obtain agreement with previous analytic results to within 0.25% at all parameter values of interest. We go on to consider irreversible and quasi-reversible systems, and demonstrate good qualitative agreement with previously described numerical and analytical results. We again make use of the FIRM and the ADI finite difference methods, and discuss when each of these methods is most appropriate.

Keywords: ADI; FIRM; Linear sweep voltammetry; Microdisc electrodes

1. Introduction

The extensive use of voltammetric techniques with microdisc electrodes has led to widespread interest in the mathematical theory underpinning such techniques [1–7]. In the case of fully reversible linear sweep voltammetry a very accurate analytical approximation has been given by Aoki et al. [2], whilst several authors have also given solutions using numerical simulation [8–16], of which the most accurate is that given by Michael et al. [8], which makes use of a conformal map in conjunction with the hopscotch algorithm. Improved versions of the conformal map technique have been given by Amatore and Fosset [9] and Verbrugge and Baker [16].

As stated by Michael et al. [8], the advantages of the numerical simulation approach is its simplicity and its flexibility, allowing a wide variety of electrochemical techniques to be investigated with only minor modifications to the numerical algorithm, whilst its major drawback in two dimensions are the heavy computing demands in terms of both CPU time and memory. In this paper we make use of the exponentially expanding mesh derived in the first paper of this series [17] to solve the problem of linear sweep voltammetry at a microdisc electrode. This mesh has been designed specifically to give a fast, efficient solution to the problem of simulation of diffusion processes at microdisc electrodes to a pre-determined level of accuracy. Michael et al. [8] gave a very comprehensive set of simulated results for each of reversible, irreversible and quasi-reversible charge transfer, and across the whole range of parameter values of interest including several cases for which no analytic solution (approximate or exact) exists. We therefore give results for a very similar set of cases in this paper, allowing direct comparison of the results obtained with the two techniques. Where possible, we

* Tel.: +44 1865 273839; e-mail: david.gavaghan@comlab.oxford.ac.uk

0022-0728/98/$ - see front matter
PII S0022-0728(98)00233-2

also compare the results of our numerical simulations to analytic results in a variety of limiting cases where analytic solutions are available, and in particular we show for reversible charge transfer that for values of the simulated current we can obtain agreement to within 0.25% of the analytic values given by Aoki et al. [2]. We again make use of both the ADI finite difference method and the fully implicit finite difference method with Richtmyer modification (the FIRM algorithm) [19–22], and we describe how the ADI algorithm can be implemented in a particularly efficient manner so that computing requirements are minimal. For most of the cases described in this paper, a complete forward sweep can be simulated using around 10–60 s (for ADI) to 1–6 min (for the FIRM algorithm) of CPU time on a computer with similar computing power (clock speed of 300 MHz) to a PC with a top-of-the-range Pentium processor.

Throughout the paper we will use the same non-dimensional constants as Michael et al. [8], since these are particularly well-suited to numerical simulation. Whenever we make comparisons to analytical work using other notations, we endeavour to explain how we have obtained the transformation.

2. The model problem

Throughout this paper, we assume that semi-infinite mass transport occurs to a disc-shaped electrode and that the electrochemical reaction

$$\mathrm{A} \pm n\mathrm{e}^- = \mathrm{B} \tag{1}$$

takes place at the disc surface. Axial symmetry allows mass transport to the electrode to be modelled by the cylindrical diffusion equation for species s

$$D_s\left(\frac{\partial^2 c_s}{\partial r^2}+\frac{1}{r}\frac{\partial c_s}{\partial r}+\frac{\partial^2 c_s}{\partial z^2}\right)=\frac{\partial c_s}{\partial t} \tag{2}$$

where r, z, represent the spatial coordinates, t is time, and $c_s(r, z, t)$ is the concentration and D_s the corresponding diffusion coefficient of each of the species $s = \mathrm{A}, \mathrm{B}$.

2.1. Boundary conditions

Assuming that the electrode potential $E(t)$ changes linearly with time and that semi infinite diffusion conditions are assumed, the following boundary and initial conditions result

$$\begin{aligned}
&z=0,\ r>a && \frac{\partial c_\mathrm{A}}{\partial z}=0 && \frac{\partial c_\mathrm{B}}{\partial z}=0\\
&z\geq 0,\ r=0 && \frac{\partial c_\mathrm{A}}{\partial r}=0 && \frac{\partial c_\mathrm{B}}{\partial r}=0\\
&z=0,\ r\leq a && D_\mathrm{A}\frac{\partial c_\mathrm{A}}{\partial z}=-D_\mathrm{B}\frac{\partial c_\mathrm{B}}{\partial z}, &\\
&D_\mathrm{A}\frac{\partial c_\mathrm{A}}{\partial z}=k_f c_\mathrm{A}-k_b c_\mathrm{B} &&&\\
&z\to\infty,\ r\geq 0 && c_\mathrm{A}=c_0 && c_\mathrm{B}=0\\
&z\geq 0,\ r\to\infty && c_\mathrm{A}=c_0 && c_\mathrm{B}=0
\end{aligned} \tag{3}$$

where a is the cathode (or electrode) radius.

The singularity arises at $r = a$, $z = 0$ due to the time-dependent discontinuity in the normal derivative at the disc edge [18]. K_f and k_b are the potential dependent rate constants for the forward and backward reactions and are given by

$$\begin{aligned}
k_\mathrm{f}&=k_0\exp\left(-\frac{\alpha nF}{RT}[E(t)-E^0]\right)=k_0\mathrm{e}^{-\alpha\tau}\\
k_\mathrm{b}&=k_0\exp\left((1-\alpha)\frac{nF}{RT}[E(t)-E^0]\right)=k_0\mathrm{e}^{(1-\alpha)\tau}
\end{aligned} \tag{4}$$

where k_0 is the heterogeneous charge transfer rate constant at standard potential E^0 and α is the charge transfer coefficient, and $E(t) = E_\mathrm{i} + vt$ with E_i the starting potential and v the sweep rate. τ is defined in Eq. (6). The nature of the charge transfer reaction at the electrode surface can be characterised by the parameter [24]

$$\Lambda=k_0\Big/\left[D_\mathrm{A}^{1-\alpha}D_\mathrm{B}^{\alpha}\left(\frac{nF}{RT}\right)v\right]^{\frac{1}{2}} \tag{5}$$

with large values of Λ corresponding to reversible charge transfer, and small values to irreversible charge transfer. Bard and Faulkner [25] give values of $\Lambda > 15$ and $k_0 > 0.3\ v^{1/2}$ cm s^{-1} for reversible, $\Lambda < 10^{-3}$ and $k_0 < 2\times 10-5\ v^{1/2}$ cm s^{-1} for irreversible, with values in between being quasi-reversible.

2.2. Non-dimensional variables

To facilitate comparison with previous work [2,8], we introduce the following non-dimensional variables

$$\begin{aligned}
&r_*=r/a && z_*=z/a\\
&u_\mathrm{A}=c_\mathrm{A}/c_0 && u_\mathrm{B}=c_\mathrm{B}/c_0 && \tau=\frac{nF}{RT}(E_i+vt-E^0)
\end{aligned} \tag{6}$$

where c_0 is the bulk concentration of species A, E^0, n, F, R and T have their usual meanings. Substitution of each of these variables into Eq. (2) gives

$$\frac{1}{p_s^2}\left(\frac{\partial^2 u_s}{\partial r_*^2}+\frac{1}{r_*}\frac{\partial u_s}{\partial r_*}+\frac{\partial^2 u_s}{\partial z_*^2}\right)=\frac{\partial u_s}{\partial \tau} \tag{7}$$

where $p_s=\left(\frac{nFa^2v}{RTD_s}\right)^{1/2}$ for $s = \mathrm{A}, \mathrm{B}$ are dimensionless parameters as introduced by Aoki et al. [2]. The boundary conditions on $r = 0$, and $z = 0$ for $r = a$ are

identical for u, whilst the others become (dropping the $*$ on r and z)

$$z=0,\ r\le a \qquad D_A\frac{\partial u_A}{\partial z}=-D_B\frac{\partial u_B}{\partial z}$$

$$\frac{\partial u_A}{\partial z}=\Lambda'[u_A e^{-\alpha\tau}-u_B e^{(1-\alpha)}]$$

$$z\to\infty,\ r\ge 0 \qquad u_A=1 \qquad u_B=0$$

$$z\ge 0,\ r\to\infty \qquad u_A=1 \qquad u_B=0 \tag{9}$$

where

$$\Lambda'=k_0a/D_A \tag{10}$$

as introduced by Michael et al. [8] is a particularly suitable non-dimensional constant for numerical simulations. It is related to the usual parameter Λ defined in Eq. (5) by $\Lambda'=p_A\Lambda$.

In the special case of equal diffusion coefficients ($D_A=D_B=D$), it is straightforward to show that $u_B=1-u_A$, and we need only solve for species A, with the corresponding simplification of the boundary conditions. Since this case has been widely investigated using both analytical [2,6,7] and simulation methods [8,9,13], most of the results presented in the next section will assume equal diffusion coefficients.

2.3. The current

The current, $I(t)$, flowing through the disc, which is the electroanalytical response function, is given by

$$I=2\pi nFD_Ac_0\int_0^a\left(\frac{\partial c_A}{\partial z}\right)_{z=0}r\ \mathrm{d}r \tag{11}$$

In dimensionless variables this corresponds to

$$\Psi=I/4nFD_Ac_0a=\frac{\pi}{2a}\int_0^1\left(\frac{\partial u_A}{\partial z}\right)_{z=0}r\ \mathrm{d}r \tag{12}$$

3. Numerical methods

In order to obtain a numerical solution the semi-infinite region $[0,\infty)\times[0,\infty)$ is replaced by the finite region $[0,r_{max}]\times[0,z_{max}]$, and we follow Britz [28] in choosing $r_{max}=1+6\sqrt{(\tau_{start}-\tau_{end})/p_{max}^2}$ and $z_{max}=6\sqrt{(\tau_{start}-\tau_{end})/p_{max}^2}$ where $p_{max}=\max(p_A,p_B)$ (since beyond this distance all concentration values will effectively equal the bulk concentration). This solution region is then discretised using a general rectangular mesh in exactly the same manner as described in the first paper of this series [17]. We described the implementation of the FIRM and ADI algorithms in the second paper of this series [27] and very similar algorithms are used here. There are two primary differences. The first is in the handling of the boundary conditions at the electrode surface, which are time dependent for linear sweep voltammetry and couple the equations for the species A and B and must therefore be treated with some care if the algorithm is to remain efficient. The second is in the timestepping algorithm: since the potential at the electrode surface is increased gradually, the transport processes are not started impulsively at time $\tau=0$, and there is therefore no initial time singularity [18,22,23,26,27]. It is not therefore necessary to use an increasing timestep, and a fixed value of $\Delta\tau$ can be used. The details of the implementations of these algorithms are given in the appendix A.

3.1. Boundary conditions

The conditions on all boundaries except the electrode surface are imposed in identical fashion to those described in the second accompanying paper for chronoamperometry [27]. The handling of the boundary conditions on the electrode surface is given in the appendix A.

3.2. Calculation of the flux

At each timestep the flux is calculated in identical fashion to that described by Eqs. (18)–(20) of the first accompanying paper [17] again making use of the trapezium rule to obtain values of the non-dimensional current ψ.

3.3. Computing

All programs used to generate results quoted in this paper are written in standard Fortran77 and were run on a Sun Workstation (Spare Ultra 30) which has a 300MHz processor. The speed of computation is therefore equivalent to a top-range PC with a Pentium processor. The codes for the FIFD and FIRM algorithms make use of routines F07 BDF and F07 BEF of the NAG Fortran Library [32], which compute the LU factorisation of a band matrix, and use this factorisation to solve the linear system, respectively, storing only the elements within the band. These routines are quite efficient in terms of both calculation and storage, and are very straightforward to use, but are not optimal for solving systems of this type [33,34]. Comparisons purely in terms of speed of computation with the ADI method, which has been optimised, are somewhat unfair. It seems likely that as the latest generation of iterative solvers [33] become more widely available, these fully implicit methods will become the methods of choice. All codes are available from the author on request.

Table 1
Convergence results for the peak current Ψ obtained by successively halving the mesh spacing h in both the r and z-directions on a regular rectangular mesh at two representative values of the nondimensional parameter ($p = 6.0$ and $p = 1.0$) assuming equal diffusion coefficients ($D_A = D_B = D$). The values given by the analytic approximation of Aoki et al. [2] are $\Psi = 2.750$ and 1.186, respectively

n_r	h	$p = 6.0$			$p = 1.0$		
		Mesh	CPU/s	Ψ	Mesh	CPU/s	Ψ
10	0.1	55×45	2	2.404	279×269	111	0.9937
20	0.05	110×90	9	2.514	557×537	478	1.049
40	0.025	219×179	58	2.585	1114×1074	2130	1.088
80	0.0125	438×358	247	2.635			

4. Results

Throughout the following, unless otherwise stated, we will consider only the case of equal diffusion coefficients, so that $D_A = D_B = D$ and $p_A = p_B = p$.

4.1. Convergence of the peak current on a mesh with constant spacing

We begin by again demonstrating the dramatic effect of the presence of the boundary singularity at the electrode edge on numerical convergence if no special techniques are used. As the test case we choose the problem of simulating fully reversible linear sweep voltammetry since for this problem we have the accurate analytic approximation of Aoki et al. [2]. Table 1 shows the convergence of the peak current for this problem on a regular rectangular mesh with fixed mesh spacing h at two representative values of the non-dimensional parameter ($p = 6.0$ and $p = 1.0$) (throughout the timings are given for 1000 timesteps of the ADI method to allow easy comparison). Parameter values are chosen to ensure a fully reversible reaction, and we have assumed equal diffusion coefficients. As was shown for chronoamperometry in the accompanying paper [27], convergence is extremely slow being accurate to only about 5 or 10% of the analytic approximation of Aoki et al. [2] on the finest mesh shown, whilst being very expensive in terms of computing time. The ratio of the errors on successive meshes is again equal to about $\sqrt{2}$, so that we might expect the exponentially expanding mesh designed to allow for the effects of the singularity [17] to give accurate results for linear sweep voltammetry.

4.2. Results using the exponentially expanding mesh

All of the results described in the rest of the paper will make use of the exponentially expanding mesh described in the first of the accompanying papers [17]. In all cases we will make use of the finer of the two meshes described there with $h_{last} = 8.0 \times 10^{-4}$ and $f = 1.175$ (giving 48 mesh points covering the electrode surface), and where possible, we will compare our simulated values with analytic approximations, and with the limiting cases of planar diffusion and steady state diffusion. We begin by considering the temporal convergence of the FIFD (fully implicit finite difference), FIRM and ADI algorithms described in the accompanying paper [27].

4.3. Temporal convergence of FIRM, FIFD and ADI

Table 2 gives the convergence of the three methods as the timestep $\Delta\tau$ is reduced. The peak flux is calculated using simple quadratic interpolation. For linear sweep voltammetry it is clear that the Richtmyer modification to the fully implicit method gives the FIRM algorithm extremely fast convergence being within 1% of the analytic solution using just 20 steps and 0.1% using just 40 timesteps, and for problems such as this where the solution does not decay with time it should be used in preference to the FIFD algorithm. The ADI method also gives very accurate values of the simulated flux using comparatively few timesteps. However, as the timestep is reduced the simulated flux continues to change as shown, although it does continue to give values accurate to better than 0.5% and eventually settles down to a similar value to that given by the FIRM algorithm. Further investigation shows this to be caused by inaccuracies in the concentration values around the singularity, which are probably caused by propagational inadequacies of the ADI method when used with larger timesteps, as compared to the fully implicit methods. This effect is more pronounced as p is reduced and we approach the steady state (this is equivalent to using increasingly large timesteps). We would therefore recommend that at least 2000 timesteps should be used with the ADI method, and that the FIRM algorithm be used for p values of less than 1.

4.3.1. Reversible charge transfer

A very accurate approximate analytic solution for the case of completely reversible charge transfer has been given by Aoki et al [2] for the case of equal diffusion coefficients. Fig. 1 (a) reproduces the results given in

Table 2
Convergence of the simulated values of the peak current with the size of the timestep used for the three solution algorithms at the two representative values of $p = 6.0$ and $p = 1.0$

n_t	$\Delta\tau$	Peak flux $p = 6.0$, Mesh $= 105 \times 57$	CPU/s	Peak flux $p = 1.0$, Mesh $= 117 \times 69$	CPU/s
FIRM algorithm					
20	1.0	2.729	22	1.1929	44
40	0.5	2.748	44	1.1865	84
80	0.25	2.749	88	1.1862	168
160	0.125	2.749	171	1.1862	332
FIFD algorithm					
20	1.0	2.762	22	1.1986	44
40	0.5	2.766	42	1.1912	85
80	0.25	2.757	85	1.1888	176
160	0.125	2.749	171	1.1875	318
ADI algorithm					
250	8×10^{-2}	2.751	1	1.1836	2
500	4×10^{-2}	2.753	2	1.1873	3
1000	2×10^{-2}	2.754	5	1.1890	8
2000	1×10^{-2}	2.753	11	1.1896	15
4000	5×10^{-3}	2.752	23	1.1896	31

The values given by the analytic approximation of Aoki et al. [2] are 2.750 and 1.186, respectively.

fig. 1 of [2] for values of p from 0.1 to 10. The solid lines are our simulated results, whilst the points were calculated using the numerical integration method suggested by Aoki et al. to evaluate eq. (6) of Ref. [2][1]. The values of the peak current and the CPU times for each value of p are given in Table 3 for both the FIRM and ADI algorithms. For the FIRM algorithm 100 timesteps were used, and for ADI 2000 timesteps, for all values of p. All values given for both simulation methods agree to within 0.25% with the analytic values of the peak flux, again confirming that the mesh derived for simulation of the steady state problem in the first paper of this series [17] is equally suited to solution of the problem of linear sweep voltammetry. The CPU times for each of the methods are quite low, requiring at most 20 s for 2000 timesteps of the ADI method, and between 1.5 and 7 min for 100 timesteps of the FIRM algorithm. This is a slightly unfair comparison since, as we showed in Table 2, the FIRM algorithm gives acceptable temporal convergence in just 50 timesteps, but for comparison with the analytic values we have chosen to present the completely converged values. In addition (as described earlier), our implementation of the FIRM algorithm makes use of off-the-shelf software packages to solve the linear system, whereas the ADI method has been coded from scratch in an optimal fashion.

As we stated earlier, the ADI method becomes increasingly inaccurate with decreasing p, since this is equivalent to approaching the steady state. Using only a small number of timesteps for near steady-state problems in non-dimensional variables is equivalent to using a very large timestep in the original dimensional variables[2], leading to stability problems with this numerical scheme, and eventually leading to oscillations in the concentration values for sufficiently small p and large $\Delta\tau$. This effect of decreasing p is also reflected in the size of the mesh required to solve the problem. As p decreases and we approach the steady state, the size of the region in which diffusion is taking place (relative to the size of the electrode) grows, and this is mirrored by an automatic growth in the size of the numerical solution region $[0, r_{max}] \times [0, z_{max}]$ as described in Section 3.

As computing power continues to increase rapidly, it is likely that the slight advantage that the ADI method currently enjoys in terms of speed will be outweighed by the advantages of the stability of the FIRM algorithm. The accuracy of the FIRM algorithm is therefore considered further in Fig. 1(b), which shows the difference (as % of peak flux) between the simulated flux values obtained using the FIRM algorithm with 100 timesteps and those obtained from the analytic method (eq. (6) of [2]). It can be seen that the maximum difference between the values for $p = 10.0$ (curve A) and $p = 1.0$ (curve G) is less than 0.05% at all values of τ. For p values between 2.0 and 4.0 the difference in-

[1] Aoki et al. did not specify an upper limit to be used in evaluating the integral, but we found (in their notation) that a value of $x = 8/p^2(20 + \zeta/2)$ gave results of the accuracy quoted by these authors. We also found that for larger values of p, 1000 divisions were required with Simpson's method to give convergence to 0.03% in the integral.

[2] For example for typical values of $D = 1 \times 10^{-9}$ m^2 s^{-1}, $a = 10$ μm, and $n = 1$, $p = 0.1$ corresponds to a sweep rate of about 0.05 V s^{-1}, giving around 10 s for the complete forward sweep.

creases to a maximum of about 0.25%, before decreasing again for $p = 6.0$ and 8.0. For $p = 0.03$ and 0.01, the simulated flux is greater than the analytic solution by up to 0.25%. These differences can be explained using the error analysis derived in the first of the accompanying papers [17]. The mesh for the simulations was derived to be optimal for electrochemical problems in the intermediate range (see section 4.5 of [17]), and was shown to overestimate the flux very slightly (by up to 0.25%) as the steady state is approached, whilst the analytic solution [2] is dependent upon the evaluation of an integral of a function which is derived by considering the limiting cases of p large and p small. The differences between analytic and simulated values for $p < 1.0$ can therefore be attributed to numerical errors in the simulated flux values, and so for $p < 1.0$ the analytic values are likely to be accurate to better than the 0.05% achieved at $p = 1.0$. It also seems likely that for $2.0 < p < 8.0$, it is the analytic values that are slightly inaccurate since we move between the limiting cases for which the analytic solution was derived, so that for $2.0 < p < 8.0$ it is the simulated values which are more accurate, again to around 0.05%. In any case, these levels of agreement are more than adequate for experimental comparison, and confirm again the accuracy of Aoki et al.'s results at all values of τ and p.

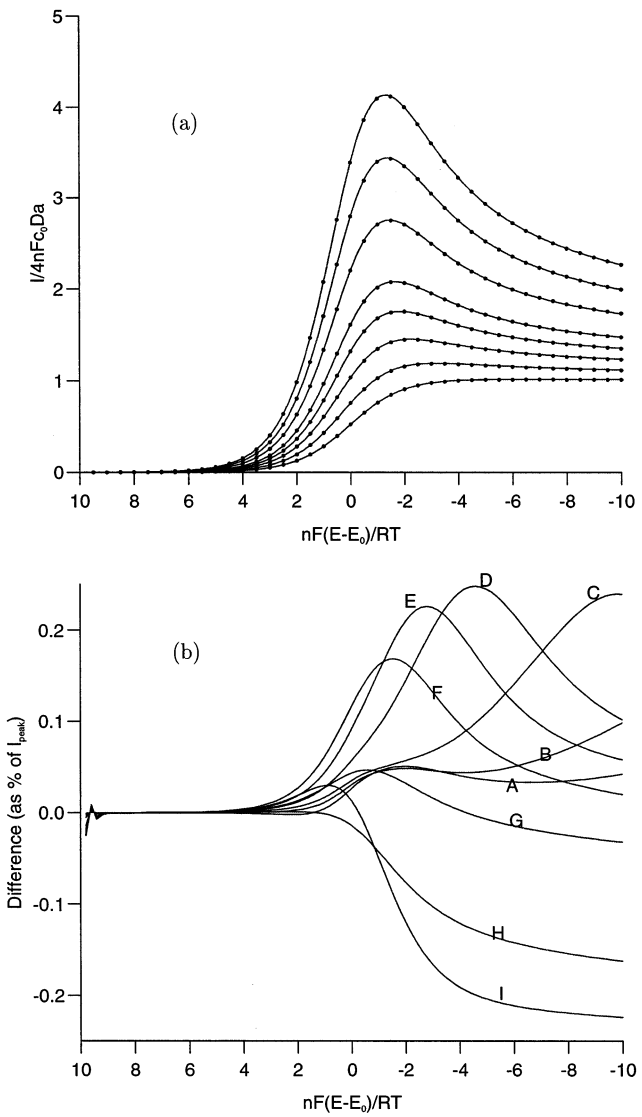

Fig. 1. (a) Comparison of the voltammograms for reversible charge transfer given by our simulations and those given using the analytic method of Aoki et al. [2]; (b) percentage difference (as % of peak flux) between simulated flux values using the analytic results given by eq. (6) of Ref [2] and the FIRM algorithm using 100 timesteps: curves A to I correspond to p values of 10, 8, 6, 4, 3, 2, 1, 0.3, and 0.1, respectively.

4.4. Some limiting cases

4.4.1. Diffusion to a planar electrode

Fig. 2 considers the limiting case as the diffusion processes tend to those for planar diffusion, as would be seen at a very large disc electrode, or when using very rapid scan rates at a smaller electrode. For example, the value of $p = 150$ (as used by Michael et al. [8]) can correspond approximately to diffusion to a disc of radius 1 mm with a scan rate of 1 V s^{-1}, or to a disc of radius 25 μm with a scan rate of 1000 V s^{-1}. The curve on the left of Fig. 2 uses a value of $\Lambda' = 10^5$ and corresponds to totally reversible charge transfer, with the points being obtained by an appropriate scaling of the values in 6.2.1 of Bard and Faulkner [25] which gives results for reversible charge transfer at a planar electrode. The curve on the right of Fig. 2 uses a value of $\Lambda' = 0.1$ and corresponds to totally irreversible charge transfer at a planar electrode, with the points being obtained by an appropriate scaling[3] of the values in table 6.3.1 of Bard and Faulkner [25] which gives results for irreversible charge transfer at a planar electrode. The level of agreement obtained is qualitatively similar to that obtained by Michael et al. (upper panel of fig. 4 of Ref. [8]). Both curves were calculated using 2000 timesteps of the ADI method.

4.4.2. Near steady state diffusion to a microdisc electrode

Bond et al. [6] and Oldham and Zoski [7] have given accurate analytic approximations for steady state voltammetry at microdisc electrodes. Oldham and Zoski [7] give the approximate analytic expression

[3] The appropriate scaling for table 6.2.1 of [25] requires that the tabulated potential values must be multiplied by $nF/\alpha RT$, and the tabulated 'current function' values by $\pi p/4$, whilst that for table 6.3.1 requires that the tabulated potential values must be multiplied by $nF/\alpha RT$ and shifted by $1/\alpha \ln[(\alpha\pi)^{1/2}/\Lambda]$, and the tabulated current values must be multiplied by $\pi p\alpha^{1/2}/4$.

Table 3
Comparison of the values of the peak current given by our simulations and those given using the analytic method of Aoki et al. [2] (with the corresponding value of τ in brackets)

p	Analytic	Peak flux ψ_{peak} (τ_{peak})				
		FIRM	CPU/s	ADI	CPU/s	Mesh
10	4.129 (−1.32)	4.127 (−1.32)	86	4.132 (−1.31)	10	102 × 54
8	3.437 (−1.36)	3.435 (−1.37)	99	3.440 (−1 37)	11	104 × 56
6	2.750 (−1.46)	2.749 (−1.46)	104	2.753 (−1.46)	11	105 × 57
4	2.079 (−1.66)	2.076 (−1.65)	125	2.080 (−1.65)	12	108 × 60
3	1.756 (−1.84)	1.752 (−1.84)	148	1.757 (−1.84)	13	110 × 62
2	1.450 (−2.22)	1.448 (−2.23)	164	1.452 (−2.22)	14	112 × 64
1	1.186 (−3.18)	1.186 (−3.19)	195	1.189 (−3.19)	10	117 × 69
0.1	1.013 (−6.68)	1.015 (−6.72)	420	1.014 (−7.4)	21	131 × 83

In all of the simulations the fine mesh with $h_{last} = 8.0 \times 10^{-4}$ and $f = 1.175$ [17] was used, with 48 points covering the electrode surface.

$$\Psi = \frac{1}{\theta}\left[1 + \frac{\pi}{\kappa\theta}\left(\frac{2\kappa\theta + 3\pi}{4\kappa\theta + 3\pi^2}\right)\right]^{-1} \quad (13)$$

where, assuming equal diffusion coefficients, $\kappa = \pi k_f a / 4D$ and $\theta = 1 + k_f/k_b$ (in terms of the nondimensional variables defined in Eq. (5) and Eq. (6), we have $\kappa = \pi\Lambda'/4 \exp(-\alpha\tau)$ and $\theta = 1 + \exp(\tau)$). Reversible steady state voltammetry corresponds to values of $\kappa \gg 1$, whilst irreversible steady state voltammetry corresponds to values of $\theta = 1$. In Fig. 3(a), we compare the results of our simulations (full lines) using a value of $p = 0.01$, which is sufficiently small for the simulation to be very close to steady state[4], with those given by Eq. (13) (points), for values of Λ' from 10 down to 0.01, covering the whole range from reversible through quasi-reversible to irreversible. Since we are dealing with near-steady state conditions, the FIRM algorithm using 100 timesteps was used to calculate each of the curves shown in Fig. 3(a), and as expected (see section 4.5 of [17]) a slight overestimation of the simulated flux can be observed at very long times (i.e. very negative values of τ). A larger mesh is also required to allow for the greater diffusion region at very long times, and all cases shown in Fig. 3(a) used a 131 × 83 mesh (again with 48 points along the electrode), and this was again determined automatically by the computer program using the criteria given in Section 3.

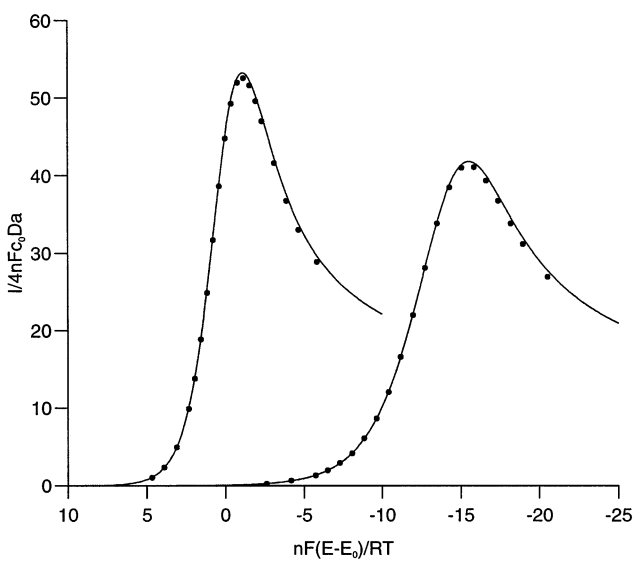

Fig. 2. Comparison of the voltammograms for a planar electrode (points obtained from Ref. [25]) with those obtained by our simulation using a value of $p = 150$.

[4] For example using the same typical values of $D = 1 \times 10^{-9}$ m^2 s^{-1}, $a = 10$ μm, and $n = 1$, $p = 0.01$ corresponds to a sweep rate of about 2.5×10^{-5} V s^{-1}.

Using the relationship between κ and τ it is straightforward to show that for the fully irreversible case, a change in the charge transfer constant from k_0 to say k_0' results in the voltammogram being shifted to the right by

$$\tau' = \frac{1}{\alpha}\ln(k_0'/k_0). \quad (14)$$

In Fig. 3(b) we have shifted each of the simulations corresponding to $\Lambda' = 10$, 3, 1, 0.3, 0.1, and 0.03 by the appropriate distance τ'. It can be seen that the curves corresponding to $\Lambda' = 0.1$ and 0.03 now lie on top of that for $\Lambda' = 0.01$ since both are very nearly irreversible, and as Λ' increases the differences in both shift and shape become more pronounced, with the rightmost shifted curve corresponding to $\Lambda' = 10$.

4.4.3. Quasi-reversible charge transfer

The remaining results presented in this paper are all qualitative, since no analytic solutions have been suggested. We therefore use 2000 timesteps of the ADI algorithm to generate the data presented in Figs. 4 and 5. Fig. 4 shows the results of simulating quasi-reversible charge transfer for which no analytical solution has yet been given. To allow comparison, we follow Michael et

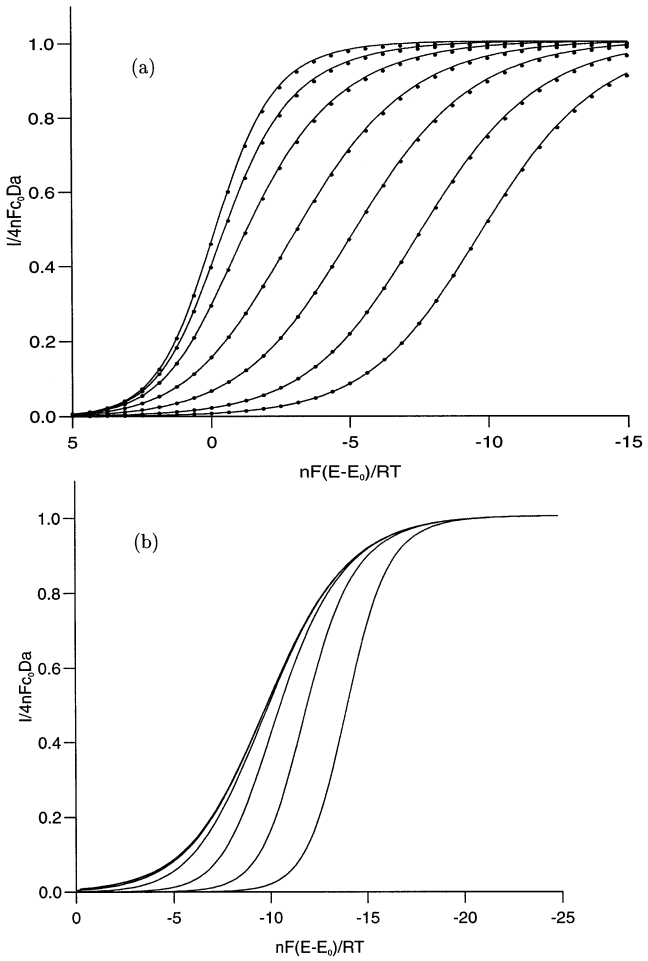

Fig. 3. (a) The steady state results for diffusion at a microdisc electrode obtained from Eq. (13) (points) and the numerical solution (line) using $p = 0.01$ and (from left to right) $\Lambda' =$ 10.0, 3.0, 1.0, 0.3, 0.1, 0.03, 0.01; and (b) the parameter values as in (a) for the numerical simulation, but with all curves shifted to the right by a distance $\tau' = 1/\alpha \ln(k'_0/k_0)$ (see Eq. (14)), with k_0 corresponding to $\Lambda' = 0.01$, so that the curves for $\Lambda' = 0.1, 0.03$ now lie on top of that for $\Lambda' = 0.01$.

al. [8] in assuming equal diffusion coefficients, and choosing values of $\alpha = 0.5$, $p = 10$, and $\Lambda =$ 10.0, 2.5, 1.0, 0.5, 0.25 and 0.1. Comparison with fig. 5 of Ref. [8] suggests that the two numerical techniques give very similar results.

4.4.4. Unequal diffusion coefficients:

Fig. 5 shows the results of our numerical simulations for reversible charge transfer with unequal diffusion coefficients. Again to allow comparison, we follow Michael et al. in choosing $p_A = 10$, with $p_B =$ 10, 5, 2.5, and 1 in Fig. 5(a), and $p_A = 1$, with $p_B =$ 10, 5, 2.5, and 1 in Fig. 5(b). In both cases the solid line shows the case where the diffusion coefficients are equal, with the curves becoming increasingly skewed as the difference between the diffusion coefficients increases. This change in shape matches that obtained by Michael et al. [8]. When considering the steady state case, Oldham and Zoski [7] found that differences in the diffusion coefficients of species A and B resulted in a potential shift equal to $\ln(D_B/D_A)$, or equivalently $\ln(p_B/p_A)^2$ (in Fig. 5(a) where $p_A > p_B$ this results in a shift to the right, and in Fig. 5(b) where $p_A < p_B$ this gives a shift to the left). All of the curves in Fig. 5 have therefore been translated along the τ (potential) axis by a distance $2\ln(p_B/p_A) = \ln(p_B/p_A)^2$. In both figures, it can be seen that for the non-steady state cases shown, the shift is a little less than $\ln(p_B/p_A)^2$, and this difference increases with the difference between the diffusion coefficients. These results are slightly at odds with those of Michael et al. who found that the shift in the potential axis was closer to $\ln(p_B/p_A)$, differing by a factor of two.

5. Discussion

In the first paper of this series [17] we derived a mesh refinement strategy which was designed to give very accurate values of the simulated flux at a microdisc electrode when using a variety of electrochemical control techniques. In this paper we have described how to use this approach to solve problems using linear sweep voltammetry at a microdisc electrode. We have followed previous authors in giving a very comprehensive set of simulated results for each of reversible, irreversible and quasi-reversible charge transfer, and across the whole range of parameter

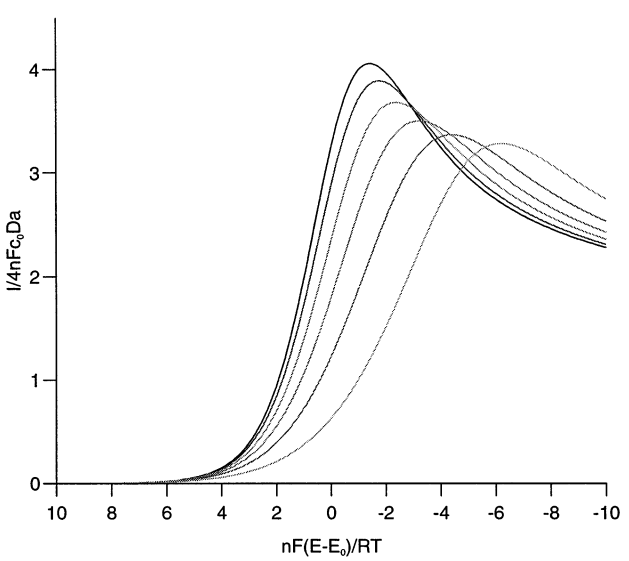

Fig. 4. The simulated voltammograms for quasi-reversible charge transfer assuming equal diffusion coefficients, $\alpha = 0.5$, with $p = 10$, and (from left to right) values of $\Lambda = 10.0, 2.5, 1.0, 0.5, 0.25$ and 0.1.

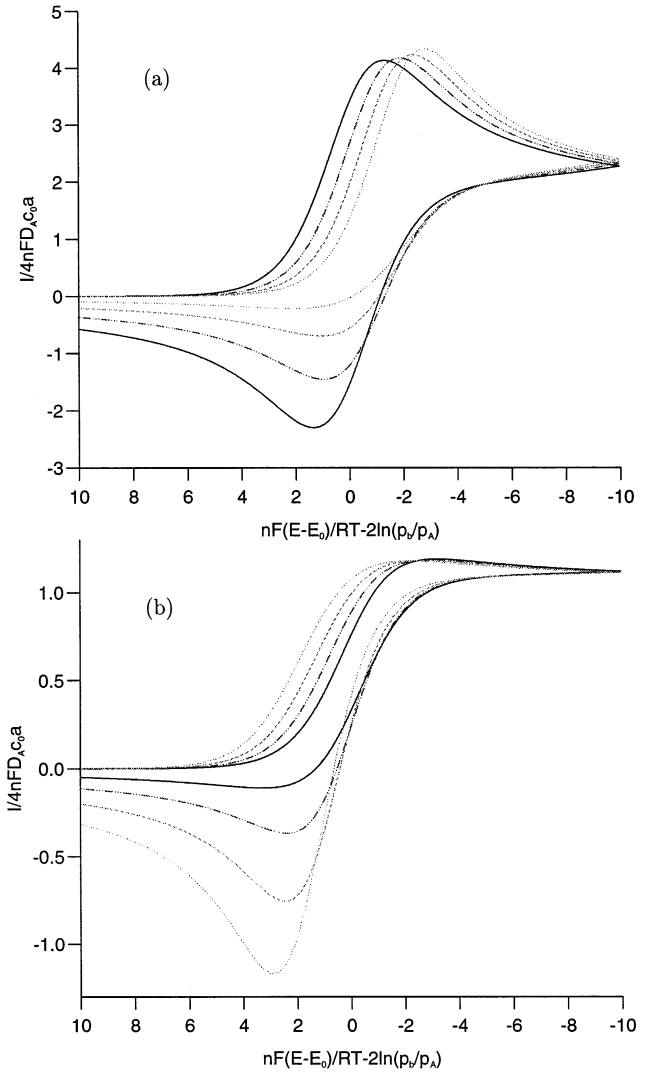

Fig. 5. The simulated voltammograms for reversible charge transfer assuming unequal diffusion coefficients. We again follow Michael et al. in choosing for (a) $p_A = 10$, with $p_B = 10, 5, 2.5$, and 1 and (b) $p_A = 1$, with $p_B = 10, 5, 2.5$, and 1. In both cases the we shift the potential axis by -2 ln (p_B/p_A) which differs from the results of Michael et al. by a factor of 2.

values of interest. Wherever possible we have compared our numerical results with analytical results and with the limiting cases of planar diffusion and steady state diffusion, and in all cases, we have shown that our simulated results give very close agreement.

6. Conclusions

In this series of introductory papers we have attempted to explain how a refined mesh can be derived which will give very accurate results for electrochemical simulations at microdisc electrodes. We have shown that over the commonly occurring experimental ranges of non-dimensional times for which the mesh is specifically designed, it is possible to achieve accuracy of around 0.1% in the simulated flux in both chronoamperometry and linear sweep voltammetry. We have also been able to use our results to explain why previous attempts at using mesh refinement have given less accurate results.

We have not made any attempt in these papers to compare this technique directly with previous approaches to the solution of two-dimensional problems in terms of either accuracy or computing speed. Typical computation costs of complete runs to near steady state for chronoamperometry, and for complete sweeps in LSV are around 1–10 min on a desk top workstation, and are therefore sufficiently fast for most purposes, and these times will decrease dramatically as the available computing power continues to increase. Mesh refinement is an extremely flexible tool which is used in other fields (particularly computational fluid dynamics) to simulate transport problems in a wide range of geometries, and our primary aim in these three papers has been to show that it can also be used to obtain accurate and computationally efficient solutions for two-dimensional electrochemical simulations. We have described its use only with finite difference methods, but it is equally applicable with finite element methods. Although we have described in these papers the use of both fully implicit (FIFD and FIRM) and semi-implicit methods (ADI), it seems likely that the greater stability of the fully implicit methods, particularly when combined with the Richtmyer modification, will make these the methods of choice for use with mesh refinement.

Mesh refinement is a very flexible tool which will allow us to model a wide range of geometries with very minor modifications to the code, and as we will show in future publications, it can be straightforwardly extended to cover the modelling of the membrane covered sensors which are commonly used in medical applications, and which are the primary motivation for our work [30,31]. It can also be extended to band, recessed and protruding electrodes and is a valuable and easy to use tool in the simulation of electrochemical processes at microelectrodes.

Acknowledgements

The author is pleased to acknowledge the financial support of the Wellcome Trust in the form of a Biomathematical Training Fellowship and a Career Development Fellowship from the Medical Research Council which has allowed him to undertake this research.

Appendix A. An efficient implementation of the ADI algorithm

As we described in the second accompanying paper [27], the ADI method can be used to obtain the solution at level $n+1$ from that at level n, by solving only tridiagonal systems in alternating directions at each half step. If we write eqs. (8) and (9) of [27] in the form

$$a_v U_{v+1} + b_v U_v + c_v U_{v-1} = d_v \qquad \text{for} \quad v = 1,\ldots,\kappa \tag{15}$$

then these become $A\mathbf{U} = \mathbf{d}$ where the matrix A has the form

$$A = \begin{pmatrix} b_1 & c_1 & & 0 \\ a_2 & & & \\ & & & c_{\kappa-1} \\ 0 & & a_\kappa & b_\kappa \end{pmatrix} \tag{16}$$

As described in [27], for the problem of chronoamperometry, there are only three distinct matrices of the form A: one associated with solving for vectors of unknowns parallel to the r-axis (corresponding to eq. (8) in Ref. [27]); and two associated with solving for vectors of unknowns parallel to the z-axis (corresponding to eq. (9) in Ref. [27]) firstly above the insulation boundary, and secondly above the electrode surface. For chronoamperometry, all of the boundary conditions are time independent ensuring that each of the matrices A are also time-independent, allowing us to decompose each of them just once into LU form before commencing the timestepping. This results in a very efficient algorithm in terms of both storage and computing time. However for voltammetry, whilst the first two forms of the matrix A remain time independent (and identical to those for chronamperometry), the third (solving for vectors of unknowns, each of length $m-1$, parallel to the z-axis and above the electrode surface) becomes time dependent, since it incorporates the time dependent boundary condition at the electrode surface. A slightly modified approach, which makes use of the Thomas algorithm [29], has therefore been adopted to maintain the speed and efficiency of the algorithm. The Thomas algorithm commences by assuming that the solution of the tridiagonal system Eq. (15) can be written in the form

$$U_{v+1} = e_{v+1} U_v + f_{v+1} \qquad \text{for} \quad v = 1,\ldots,m-1 \tag{17}$$

Substituting this into Eq. (15) for U_{v+1} and comparing coefficients gives

$$e_v = \frac{-a_v}{b_v + c_v e_v + 1} \quad \text{and} \quad f_v = \frac{d_v - c_v f_{v+1}}{b_v + c_v e_{v+1}} \quad \text{for} \quad v = 1,\ldots,m-1. \tag{18}$$

Since the value on the far field boundary is known ($U_m = 1$), and if we also assume $U_{m+1} = 1$ giving $e_m = 1$ and $f_m = 0$, then we can then solve recursively for e_v and f_v for $j = m-1,\ldots,1$.

A.1. Case 1: Equal diffusion coefficients

In the special case of equal diffusion coefficients the boundary condition at the electrode surface (see Eq. (9)) reduces to

$$\text{On} \quad z = 0,\ r \le a,$$

$$\frac{\partial u_A}{\partial z} = \Lambda'[u_A e^{-\alpha\tau} - (1-u_A)e^{(1-\alpha)\tau}] \tag{19}$$

Replacing the partial derivative by the appropriate second order finite difference representation with $u_A \approx U$ (see eq. (29) of [17]) gives

$$-\frac{k_0^2 U_{i,2} - (k_0+k_1)^2 U_{i,1} - (k_1^2 + 2k_0k_1)U_{i,0}}{k_0 k_1 (k_0+k_1)} = \Lambda'[U_{i,0}e^{-\alpha\tau} - (1-U_{i,0})e^{(1-\alpha)\tau}] \tag{20}$$

where k_0, k_1 are the first two mesh spacings in the z-direction. For each i, we can then use the appropriate equations for $U_{i,2}$ and $U_{i,1}$ from the Thomas algorithm Eq. (17), giving three equations in three unknowns which can be solved straightforwardly to obtain $U_{i,0}$, and hence $U_{i,j}$ for $j = 1,\ldots,m-1$ again from Eq. (17). This process is repeated for each $i = 1,\ldots,n_r$.

A.2. Case 2: Unequal diffusion coefficients

In the case of unequal diffusion coefficients, we must solve for both species A and B simultaneously. In this case, we replace the partial derivatives in the boundary conditions at the electrode, Eq. (9) by their finite difference representations in the same way as in Eq. (20) above. This gives two equations involving the six unknowns $U^A_{i,j}$, $U^B_{i,j}$, $j = 0, 1, 2$, for each of the $i = 1,\ldots,n_r$ vectors above the electrode. From the Thomas algorithm, for each species we then obtain the four equations

$$U^A_{i,2} = e^A_{i,2} U^A_{i,1} + f^A_{i,2} \qquad U^A_{i,1} = e^A_{i,1} U^A_{i,0} + f^A_{i,1}$$

$$U^A_{i,2} = e^B_{i,2} U^B_{i,1} + f^B_{i,2} \qquad U^B_{i,1} = e^B_{i,1} U^B_{i,0} + f^B_{i,1}.$$

Combining these four equations with the finite difference representations of the boundary conditions at the electrode surface, gives six equations in six unknowns which can be solved by matrix inversion. These can then be used in conjunction with Eq. (17) to solve for the rest of the unknown values of $U^A_{i,j}$, $U^B_{i,j}$, $j = 3,\ldots,m-1$. This process is carried out for each of the $i = 1,\ldots,n_r$ vectors above the electrode on each timestep.

References

[1] R.S. Nicholson, I. Shain, Anal. Chem. 36 (1964) 707.
[2] K. Aoki, K. Akimoto, K. Tokuda, H. Matsuda, J. Electroanal. Chem. 171 (1984) 219.
[3] M. Fleischmann, J. Daschbach, S. Pons, J. Electroanal. Chem. 250 (1988) 269.
[4] C.G. Phillips, J. Electroanal. Chem. 333 (1992) 11.
[5] D.R. Baker, M.W. Verbrugge, J. Electrochem. Soc. 137 (1990) 1832.
[6] A.M. Bond, K.B. Oldham, C.G. Zoski, J. Electroanal. Chem. 245 (1988) 71.
[7] K.B. Oldham, C.G. Zoski, J. Electroanal. Chem. 256 (1988) 11.
[8] A.C. Michael, R.M. Wightman, C.A. Amatore, J. Electroanal. Chem. 267 (1989) 33.
[9] C.A. Amatore, B. Fossett, J. Electroanal. Chem. 293 (1990) 19.
[10] J. Galceran, D.J. Gavaghan, J.S. Rollett, J. Electroanal. Chem. 394 (1995) 17.
[11] D.J. Gavaghan, J.S. Rollett, J. Electroanal. Chem. 295 (1990) 1.
[12] J. Heinze, J. Electroanal. Chem. 124 (1981) 73.
[13] J. Heinze, M. Storzbach, Ber. Bunsenges. Phys. Chem. 90 (1986) 1043.
[14] D. Shoup, A. Szabo, J. Electroanal. Chem. 140 (1982) 237.
[15] D. Shoup, A. Szabo, J. Electroanal. Chem. 160 (1984) 1.
[16] M.W. Verbrugge, D.R. Baker, J. Phys. Chem. 96 (1992) 4572.
[17] D.J. Gavaghan, J. Electroanal. Chem. 456 (1998) 1.
[18] D.J. Gavaghan, J. Electroanal. Chem. 420 (1997) 147.
[19] M. Rudolph, J. Electroanal. Chem. 314 (1991) 13.
[20] M. Rudolph, J. Electroanal. Chem. 338 (1995) 85.
[21] J. Mocak, S.W. Feldberg, J. Electroanal. Chem. 378 (1994) 31.
[22] S.W. Feldberg, C.I. Goldstein, J. Electroanal. Chem. 397 (1995) 1.
[23] D. Britz, J. Heinze, J. Mortensen, M. Storzbach, J. Electroanal. Chem. 240 (1988) 27.
[24] H. Matsuda, Y. Ayabe, Z. Elektrochem. 59 (1955) 494.
[25] A.J. Bard, L.R. Faulkner, Electrochemical Methods, Wiley, New York, 1980.
[26] C.E. Pearson, Math. Comput. 19 (1965) 570.
[27] D.J. Gavaghan, J. Electroanal. Chem. 456 (1998) 13.
[28] D. Britz, Digital Simulation in Electrochemistry, 2nd edition, Springer, Heidelberg, 1988.
[29] K.W. Morton, D.F. Mayers, Numerical Solution of Partial Differential Equations, Cambridge University Press, Cambridge, 1994.
[30] L. Sutton, D.J. Gavaghan, C.E.W. Hahn, J. Electroanal. Chem. 408 (1996) 21.
[31] C.E.W. Hahn, H. McPeak, A.M. Bond, J. Electroanal. Chem. 393 (1995) 69.
[32] The NAG Fortran Library Manual–Mark 16, The Numerical Algorithms Group Limited, Oxford, (1993).
[33] J.A. Alden, R.G. Compton, J. Phys. Chem. B 101 (1997) 8941.
[34] J.A. Alden, R.G. Compton, J. Phys. Chem. B 101 (1997) 9606.